Journal of Materials Chemistry C

Accepted Manuscript

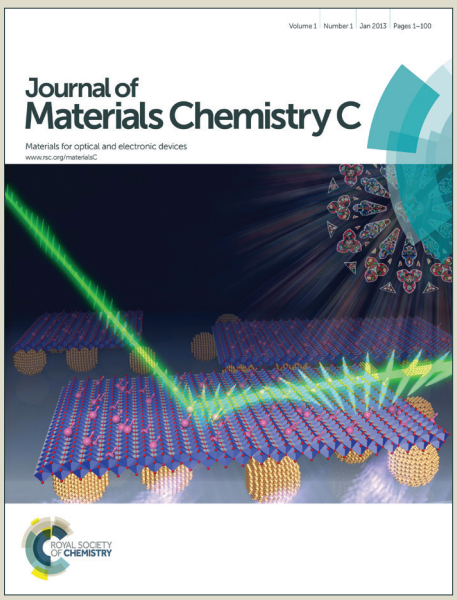

ROYAL SOCIETY OF CHEMISTRY

www.rsc.org/materialsC

ARTICLE Journal Name

New solid-state Eu(III)-containing metallo-supramolecular polymers: Morphology control and optical wave-guiding properties

Cite this: DOI: 10.1039/x0xx00000x

Received ooth January 2012,
Accepted ooth January 2012

DOI: 10.1039/x0xx00000x

www.rsc.org/

Andre Duerrbeck,[a,b,c] Sergey Gorelik,[b] Jonathan Hobley,[d] Anna Marie Yong,[b] Gomathy Sandhya Subramanian,[b] Andy Hor[a,b*] and Nicholas Long[c*]

Herein, we report the solution phase self-assembly between Eu(III) and a rigid ditopic tridentate terpyridine ligand which results in the formation of supramolecular metallo-networks in the solid state. Depending on the ligand to metal ratio used for the initial self-assembly process, the morphology of these materials can be altered from one-dimensional micron-sized fibres to a three-dimensional coordination network. The terpyridine-based ditopic ligand can act as an efficient sensitizer for Eu(III) emission whereby the emission lifetimes and ligand triplet state energies of the metallo-polymers strongly depend on the ligand to metal ratio. The obtained micron-sized fibres can act as an efficient optical wave-guide for Eu(III) emission.

Introduction

Within the area of supramolecular chemistry the research in the field of supramolecular polymers, where small molecules are linked together by weak and reversible non-covalent bonds has greatly increased in recent years.[1] These non-covalent interactions can range from hydrophobic interactions,[2] π-π-stacking,[3] hydrogen bonding,[4] or metal ion coordination.[5] Coordinative interactions can be used for the formation of metallo-supramolecular polymers where a metal-induced self-assembly process between metal ions and an organic linker results in the formation of large polymeric structures.[6] The advantage of these metallo-polymers is that they combine the mechanical properties of conventional covalently-bound polymers with the unusual features introduced by the metal ions such as magnetic,[7] electrochromic,[8] optical,[9] or catalytic properties.[10] The strength of the coordination interaction between the organic ligand and the metal ions determines whether the resulting metallo-polymers can be considered as kinetically labile or stable.[11] If the binding constants are strong the self-assembly process will continue until the assembly reaches a critical mass and precipitates as an insoluble material. On the other hand, if the binding constants are weak the competitive coordination of solvent molecules limits the self-assembly process and as a result the formation of larger assemblies will be minimized. If the binding constants lie within these two possibilities it is possible to achieve the formation of soluble dynamic coordination polymers which can show promising self-healing and stimuli-responsive properties.[12] Next to the metal ion used for the self-assembly the choice of the ligand plays an important role on the stability of these metallo-supramolecular polymers. A typical ligand usually consists of two coordinating motifs which are linked together by a rigid organic spacer. One of the most common coordinating types used is the NNN-coordinating terpyridine moiety because of their good binding properties to a wide range of transition metals.[13] Typical spacers are phenyl and biphenyl but other spacers such as perylene bisimide dyes have also been used to introduce new optical properties.[14] In order to achieve the formation of linear one-dimensional polymeric chains these rigid ditopic tridentate ligands must coordinate to hexacoordinate transition metal ions such as Ru(II), Zn(II), Fe(II), or Co(II). The size of these coordination polymers strongly depends on the ligand to metal ratio and ideally should be close to 1:1. Small deviations from this ratio result in the formation of shorter oligomers instead of longer polymeric chains. Also the binding constant for the coordination of the second ligand to the metal should be higher than for the coordination of the first ligand since the second binding constant determines the growth of the coordination polymers in solution. However, while the size of the coordination polymers can be altered by concentration and ligand to metal ratio, the one-dimensional morphology of these metallo-polymers cannot be altered due to the rigidity of the ligand. One way to overcome this problem is to use a flexible chain instead of a rigid conjugated system as spacer but the flexibility of the resulting ligand during a metal-induced self-assembly process can lead to the formation of rings rather than polymeric structures which limits their potential for the preparation of coordinative polymers with a high molecular weight. Another way to achieve a controllable morphology change is the use of tritopic ligands with three coordinating sites. This approach was recently further extended by using a mixture of ditopic and tritopic ligands which led to the formation of branched transition metal metallo-polymers in the solid state.[15] A further approach to alter the metallo-polymer morphology is the incorporation of lanthanide ions instead of transition metals. Due to the larger ionic radius compared to transition metals, lanthanide ions can coordinate up to three ditopic tridentate ligands and thus usually result in the formation of three-dimensional polymeric networks rather than one-dimensional polymeric chains. Furthermore, lanthanides (especially Eu(III) and Tb(III)) offer outstanding photophysical properties such as narrow band emission lines, long lifetimes, and high quantum yields.[16] However, f-f-transitions are parity forbidden and as a result lanthanide ions show very low molar absorption coefficients. This problem can be overcome by coordinating lanthanide ions to an organic ligand which can act as a sensitizer for Ln(III) emission whereby the organic ligand absorbs light and transfers energy via the ligands triplet state to the Ln(III) centre from where the metal centred emission occurs. One example of a ligand which can act as an efficient for Ln(III) emission sensitizer in solution as well as in the solid state is the tridentate terpyridine ligand.[17,18] It has been shown that supramolecular

coordination networks can be achieved in solution by a self-assembly process between Ln(III) ions and ditopic ligands and can result in the formation of dynamic stimuli-responsive materials.[12] Furthermore, it has been found that the concentration, ligand to metal ratio as well as the ligand flexibility plays an important role on the morphology of the coordination network in solution, whereby changes from a branched network to polymeric rings can be achieved.[19] However, compared to studies of morphology controllable self-assembled supramolecular Ln(III) coordination networks in solution, their properties have been rarely studied in the solid state. To further extend the knowledge in this area, we herein report the formation of emissive Eu(III) based metallo-supramolecular polymers with a solid state controllable morphology.

Experimental

Materials

All commercially obtained chemicals were used as received without any further purification. $Eu(NO_3)\cdot 5H_2O$ was stored in a glovebox under controlled atmosphere. All solvents were of HPLC grade. If not otherwise stated, all synthetic procedures and measurements were carried out at room temperature.

Synthesis of ligand 1

The terpyridine-based ditopic ligand was prepared according to a modified reported literature three step synthetic procedure.[20,21]

(2E,2'E)-3,3'-(1,4-phenylene)bis(1-(pyridin-2-yl)prop-2-en-1-one) (1a) Terephthalaldehyde (1.8 g, 13.42 mmol, 1 eq) was added to a mixture of potassium hydroxide (1.5 g, 26.84 mmol, 2 eq) in water (10 mL) and methanol (250 mL). After complete dissolution, 2-acetylpyridine (3 mL, 26.84 mmol, 2 eq) was added and a yellow precipitate occurred. The resulting suspension was left stirring for two days at room temperature. Afterwards the precipitate was filtered off, washed with methanol, and dried in air overnight. The desired product was obtained as a yellow solid (3.44 g, 10.11 mmol, 75%). ^{1}H NMR (400 MHz, $CDCl_3$): δ (ppm) = 7.50 (dd, 2H, $^3J_{HH}$ = 7.84, 4.58 Hz, N-CH=C*H*-CH=CH-C), 7.77 (s, 4H, Py*H*), 7.89 (dd, 2H, $^3J_{HH}$ = 7.90, 7.80 Hz, N-CH=CH-C*H*=CH-C), 7.93 (d, 2H, $^3J_{HH}$ = 16.05 Hz, OC-C*H*=CH), 8.20 (d, 2H, $^3J_{HH}$ = 7.86 Hz, N-CH=CH-CH=C*H*-C), 8.35 (d, 2H, $^3J_{HH}$ = 16.11 Hz, OC-CH=C*H*), 8.75 (d, 2H, $^3J_{HH}$ = 4.77 Hz, N-C*H*=CH-CH=CH-C). ^{13}C NMR (100 MHz, $CDCl_3$): δ (ppm) = 122.0, 123.12, 127.14, 129.41, 137.21, 137.32, 143.72, 149.04, 154.24, 189.47. ES+ TOF HRMS ($CHCl_3$): *m/z* 341.1303 $[M + H]^+$ (calc. for $C_{22}H_{17}N_2O_2^+$ 341.1285).

1,4-Bis[1,5-dioxo-1,5-bis(2-pyridyl)pentan-3-yl]benzene (1b) A mixture of (2E,2'E)-3,3'-(1,4-phenylene)bis(1-(pyridin-2-yl)prop-2-en-1-one) (3 g, 8.81 mmol, 1 eq), 2-acetylpyridine (2.16 g, 9.39 mmol, 2.2 eq) and potassium hydroxide (1.09 g, 19.39 mmol, 2.2 eq) in water (10 mL) and ethanol (250 mL) was set to reflux overnight and allowed to cool to room temperature afterwards. The resulting dark red solution was filtered and the obtained solid was washed several times with ethanol to give the desired product as a white solid (3.39 g, 5.81 mmol, 66 %). ^{1}H NMR (500 MHz, $CDCl_3$): δ (ppm) = 3.61 (d, 8H, $^3J_{HH}$ = 6.94 Hz, C*H*$_2$), 4.09 (q, 2H, $^3J_{HH}$ = 7.01 Hz, Ph-C*H*-(CH$_2$)$_2$), 7.29 (s, 4H, Ph*H*), 7.43 (dd, 4H, $^3J_{HH}$ = 7.41, 4.80 Hz, N-CH=C*H*-CH=CH-C), 7.79 (dd, 4H, $^3J_{HH}$ = 7.23, 8.09 Hz, N-CH=CH-C*H*=CH-C), 7.94 (d, 4H, $^3J_{HH}$ = 8.01 Hz, N-CH=CH-CH=C*H*-C), 8.63 (d, 4H, $^3J_{HH}$ = 4.79 Hz, N-C*H*=CH-CH=CH-C). ES+ TOF HRMS ($CHCl_3$): *m/z* 583.2353 $[M + H]^+$ (calc. for $C_{36}H_{31}N_4O_4^+$ 583.2340), 605.2164 $[M + Na]^+$ (calc. for $C_{36}H_{30}N_4NaO_4^+$ 605.2159).

1,4-Bis(2,2':6',2''-terpyridine-4'-yl)benzene (ligand 1)
A suspension of 1,4-bis[1,5-dioxo-1,5-bis(2-pyridyl)pentan-3-yl]benzene (1 g, 1.72 mmol) and ammonium acetate (5 g) in abs. ethanol (50 mL) was heated to reflux for 5 days and cooled to room temperature afterwards. The precipitate was filtered off and washed with ethanol to yield the desired product as an off-white solid (0.67 g, 1.24 mmol, 72 %). The product was further purified by recrystallization from glacial acid which was repeated for five times. ^{1}H NMR (500 MHz, $CDCl_3$): δ (ppm) = 7.38 (dd, 4H, $^3J_{HH}$ = 8.79, 4.75 Hz, N-CH=C*H*-CH=CH-C), 7.90 (dd, 4H, $^3J_{HH}$ = 8.49, 7.92 Hz, N-CH=CH-C*H*=CH-C), 8.07 (s, 4H, Ph*H*), 8.69 (d, 4H, $^3J_{HH}$ = 7.97 Hz, N-CH=CH-CH=C*H*-C), 8.76 (d, 4H, $^3J_{HH}$ = 4.69 Hz, N-C*H*=CH-CH=CH-C), 8.81 (s, 4H, Ph-Py*H*). ES+ TOF HRMS ($CHCl_3$): *m/z* 541.1641 $[M + H]^+$ (calc. for $C_{36}H_{25}N_6^+$ 541.2136), 271.0865 $[M + 2H]^{2+}$ (calc. for $C_{28}H_{26}N_6^{2+}$ 271.1104). Elemental Analysis (540.62 g/mol) found: C 79.82, H 4.25, N 15.38, expected: C 79.98, H 4.47, N 15.55

Preparation of metallo-supramolecular polymers

For the preparation of the metallo-supramolecular polymers in a ligand to metal ratio of 1:1, $Eu(NO_3)_3\cdot 5H_2O$ (0.1 mmol) was dissolved in a mixture of acetonitrile and chloroform (v:v / 1:1, 200 mL in total). Ligand **1** (0.1 mmol) in chloroform (100 mL) was sonicated until complete dissolution. The resulting solution was added dropwise under vigorous stirring to the solution of $Eu(NO_3)_3$ at room temperature. After complete addition the resulting solution was allowed to evaporate slowly under an atmosphere of nitrogen. After several hours an off-white precipitate appeared which was filtered off and washed several times with chloroform and acetonitrile. The resulting powder was dried under vacuum overnight. For the metallo-supramolecular polymers in a ligand to metal ratio of 2:1 and 3:1, the amount of ligand added was adjusted to 0.2 mmol and 0.3 mmol respectively while the other parameters remained constant. The obtained yields were 92% (ligand to metal ratio 1:1), 81% (ligand to metal ratio 2:1), and 63% (ligand to metal ratio 3:1).

Instrumentation and methods

NMR spectra were recorded on a Bruker 400 MHz and on a JEOL 500 MHz spectrometer. High resolution mass spectra were recorded on a Shimdazu LCMS-IT-TOF Liquid Chromatograph Mass Spectrometer. Samples for mass spectra had a concentration of about 1 x 10^{-4} M and were filtered through a 0.2 µm syringe filter prior to injecting into the spectrometer. Elemental analysis was performed on a Thermo Scientific Elemental Analyzer (Flash 1112 Series) with a typical sample amount of around 2 mg. Thermogravimetic analysis was carried out on a TGA Q500 (TA Instruments) using an alumina sample pan. The quantity per sample for a typical experiment was around 10 mg. The experiments were performed under nitrogen gas with a flow rate of 60 ml/min. Samples were heated up from room temperature to 800 °C with a ramp rate of 10 °C/min. Elemental analysis was performed by X-ray photoelectron spectroscopy on a Thermo Fischer Scientific Theta Probe XPs with an Al K alpha monochromatic X-ray source with survey scan pass energy of 200 eV and high resolution scan pass energy of 40 eV. Microscope slides (Sail Brand Cat. No. 7101) were cut to an approximate size of 1x1 inch and were sonicated in soap (Hellmanex II), DI water, acetone, methanol, iso-propanol (20 min each) and dried at 100 °C overnight. Prior to spin-coating the glass slides were further treated under a Novascan PSD-UVT UV Ozone cleaner for 15 min at room temperature. Spin-coated samples were prepared using a Headway Research Inc. spin coater (model PWM32). Typical spin coating parameters were set to a speed of 4000 rpm, speed ramp of 1000 rpm/sec and time of 50 sec. SEM images were obtained on a JEOL FESEM JSM6700F instrument with an accelerating voltage of 15 kV using an in-lens detector at a working distance of 7 mm.

EDX maps were obtained on JEOL FEG-SEM JSM-7600F equipped with an Oxford Aztec Energy System. Samples for SEM were sputtered with gold using a JEOL JFC-1200 Fine Coater. A typical sputtering time for the coating was about 50 sec per sample. Europium emission microscope images were taken using a wide-field fluorescence microscope consisting of an inverted Nikon Eclipse Ti microscope equipped with an Andor Shamrock spectrograph and Andor Newton ICCD camera. A Xe lamp with a set of appropriate optical band-pass filters was used as excitation source (λ_{ex} = 330 – 380 nm). Optical microscope images were taken in transmission mode using a Xe lamp as a light source, dark field condenser and an Andor IXONt camera (40x objective). Time-resolved emission spectroscopy measurements were carried out using an Edinburgh Instruments flash-photolysis spectrometer LP920 equipped with an Edinburgh Instruments LP920-K PMT detector and a time-gated Andor DH720 ICCD camera. The maximum time resolution of the setup was 10 ns. Samples were excited at 355 nm using a 3rd harmonic of Nd-YAG laser of an Expla NT341A OPO laser system. The excitation pulse energy was about 1 mJ, within a beam diameter of about 5 mm. Measurements at 77 K were performed using an Oxford Instruments DN2 optical cryostat with a Mercury iTC temperature controller. The cooling rate for a typical experiment was about 0.05 K/sec. All photophysical data reported herein are the average of three independent measurements. Samples obtained in a ligand to metal ratio of 2:1 were tested for wave-guiding properties using a Witec alpha 300R Raman microscope with a CCD camera mounted onto the eyepiece. A DPSS CW-355 nm laser light was coupled into the microscope using a single mode optical fibre and focused onto the sample using a 40x (Nikon S Plan Fluor, 0.6 N.A) objective. Images of Eu(III) emission were taken using a 355 nm cut-off edge long-pass optical filter. Optical images were taken without the 355 nm edge filter.

Results and discussion

Ligand **1** can be obtained via a three step synthetic pathway (Scheme 1).[20,21]

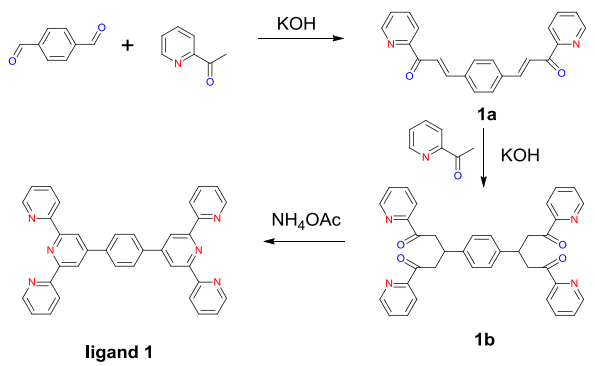

Scheme 1: Synthetic pathway to obtain ligand 1.

The first step is an aldol condensation between terephthalaldehyde and 2-acetylpyridine with potassium hydroxide as base to form the E-configurated conjugated enone 1a. The second step is a Michael addition with 2-acetylpyridine and potassium hydroxide as base which resulted in the 1,5-dicarbonyl compound 1b. It should be noted that in the previous literature procedure, both steps can be carried out in a one-pot reaction. However, we noted that the yield can be increased if the first product is purified before further treatment with 2-acetylpyridine. The final step to obtain ligand **1** is the formation of the centre pyridine ring with ammonium acetate. In addition to previous literature procedures the ligand was further purified by recrystallization from glacial acid. The overall yield after three steps was 36%.

Preparation of metallo-supramolecular polymers

The Eu(III) containing metallo-supramolecular polymers were prepared by a metal ion induced self-assembly process at room temperature in a chloroform / acetonitrile solvent mixture. We found that in order to achieve a controlled self-assembly process, the total volume of the solvent mixture as well as the slow dropwise addition of the ligand to the metal ions plays an important role. If the total volume of the chloroform/acetonitrile solvent mixture was too low a precipitate was formed upon addition of the ligand. The same effect took place if the ligand was added to the metal in large quantities. We found that the resulting precipitate, which displayed bright red luminescence upon UV-excitation, indicating the formation of metal coordination complex, consisted of small aggregated particles without a specific morphology. We expect that under these conditions no controlled self-assembly in solution occurred and that small particles were formed initially which then aggregated and precipitated. Therefore the conditions were changed to a relatively large total volume of the solvent mixture and a slow dropwise addition of ligand. A partial slow evaporation of the solvent then led to the formation of an insoluble precipitate which was filtered off and washed several times with acetonitrile and chloroform to remove all soluble residues as well as potential uncoordinated ligand.

Elemental composition

Due to the dynamic self-assembly process in solution and the insolubility of the resulting metallo-polymers, it is rather difficult to obtain a detailed structural analysis of the samples prepared herein. Several attempts were made to obtain single crystals but in all cases only the formation of an amorphous solid was observed. This drawback has also been observed by other groups who studied metallo-polymers based on similar ligands and transition metals.[9] In order to get a deeper insight into the elemental composition of the metallo-polymers at different ligand to metal ratios, CHN and thermogravimetric analysis as well as elemental analysis using XPS were carried out.

Table 1: Results from elemental analysis and calculated weight loss of organic ligand from TGA for the metallo-supramolecular polymers in different ligand to metal ratios.

	1:1	**2:1**	**3:1**
C / wt%	32.86	39.06	43.75
H / wt%	2.37	2.78	3.04
N / wt%	11.50	10.94	11.07
TGA weight loss / wt%[(a)]	33	42	44

[(a)]Corrected by weight loss of solvent.

The weight loss profiles for the uncoordinated ligand **1** as well as the Eu(III) metallo-polymers in different ligand to metal ratios are represented in Figure 1. The uncoordinated ligand shows a single sharp decomposition line at around 450 °C. In comparison, the Eu(III) containing metallo-polymers show two

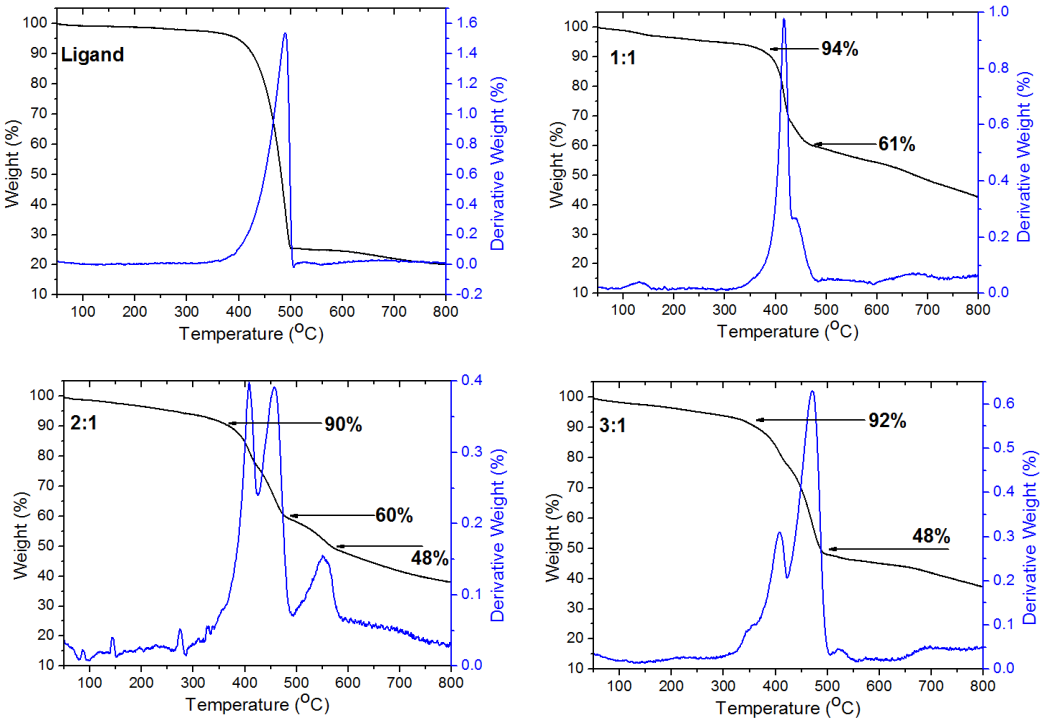

Figure 1: Thermogravimetric analysis of the uncoordinated ligand 1 and the Eu(III) containing metallo-supramolecular polymers in different ligand to metal ratios.

or three decomposition lines between around 420 °C and 550 °C which is assumed to result from coordinated ligand. From the weight loss profiles the weight percentage of coordinated ligand (corrected by the weight loss of solvent molecules in the samples) can be calculated and showed that the weight percentage of coordinated ligand increases from about 33% at a ligand to metal ratio of 1:1 to about 44% at a ligand to metal ratio of 3:1 (Table 1).

Table 2: Results from elemental analysis made by XPS and the calculated Eu : C atom ratios as well as the estimated number of coordinated ligand present in the samples at different ligand to metal ratios.

	1:1	2:1	3:1
C / at%	67.72	74.89	75.10
N / at%	11.16	10.77	10.51
O / at%	19.27	13.18	13.56
Eu / at%	1.87	1.16	0.83
Eu : C[(a)]	1 : 36.21	1 : 64.56	1 : 90.48
Coordinated Ligands[(b)]	1.01	1.79	2.51

[(a)]Ratio of europium to carbon atoms calculated from obtained XPS at%, [(b)]estimated number of coordinated ligands from the Eu:C ratio (one ligand corresponds to 36 carbon atoms).

To confirm that the weight loss resulted from carbon atoms from the coordinated ligand, CHN elemental analysis was carried out. The results from CHN elemental analysis show a similar trend obtained by TGA in that with higher ligand to metal ratios the carbon content of the samples increases (Table 1). The obtained weight percentages of carbon in all samples are in relatively good agreement with the calculated weight loss from TGA indicating that that the main mass loss from TGA corresponds to the decomposition of ligand in the samples. Further elemental analysis was obtained by X-ray photoelectron spectroscopy (Table 2).

For all three samples the presence of europium could be confirmed. Since we have shown that the carbon content in the samples mainly comes from coordinated ligand, it is possible to calculate the ratio of the atomic percentages of ligand carbon atoms to one europium metal atom. Furthermore, since one ligand has 36 carbon atoms, the number of coordinated ligands to one Eu(III) metal centre can be estimated and shows that the amount of coordinated ligand increases from around 1.0 to 1.8 and 2.5 with increases in the ligand to metal ratio of 1:1 to 2:1 and 3:1 respectively. It should be noted that the formation of Ln(III) based coordination polymers with related ditopic ligands in solution showed that the experimental value for the ligand to metal ratio with the highest degree of a network formation 1.5:1.[19,22] The values for the ligand to metal ratio for the metallo-polymers reported herein are slightly higher than expected for a formation of one-dimensional polymeric or three-dimensional network structures, especially for the sample in a ligand to metal ratio of 3:1. It should be noted that the elemental results from XPS are not corrected for the presence of solvent molecules in the sample which has been shown to account for around 10 wt% in each sample. Therefore the exact ligand to metal ratio might be slightly lower than the one calculated from XPS elemental analysis. However, the XPS results confirmed the findings made by TGA that an increased concentration of ligand in solution during the self-assembly process leads to the coordination of more ligand relative to Eu(III) and thus results in higher ligand to metal ratios in the solid state. Since the weight percentage of solvent molecules is similar for all three samples the relative ligand to metal ratio made by XPS should not be affected.

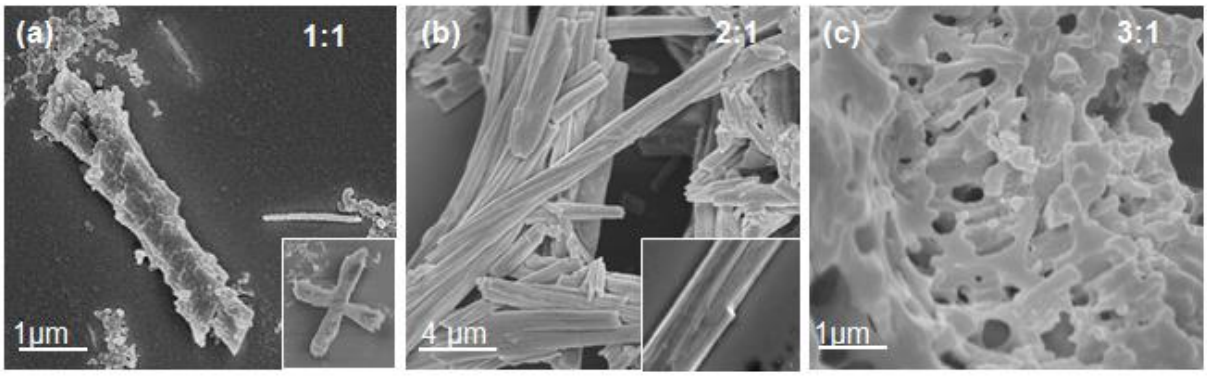

Figure 2: SEM images of the samples in the solid state: (a) ligand to metal ratio 1:1, (b) ligand to metal ratio 2:1, (c) ligand to metal ratio 3:1.

Morphology

The morphology of all the Eu(III) containing samples was firstly investigated by scanning electron microscopy (SEM). In order to observe individual particles all samples were dispersed and sonicated in a chloroform solution and spin-coated onto a glass slide. The SEM images show significant changes in the morphology of the coordination polymers upon changing the ligand to metal ratio (Fig. 2). For simplicity we will refer to the ligand to metal ratio in solution used for the self-assembly process even though the exact ratio in the solid state differs from that initial ligand to metal ratio.

In case of an equal ligand to metal ratio of 1:1, the formation of three different morphologies can be observed in a typical SEM image. The majority of the sample consists of short and broad micron-sized rods with an average length of about 3 µm and an average width of about 0.5 µm. The other species consist of either short and thin micron-sized fibres or particles without any specific shape. Interestingly another favoured shape is the formation of cross-shaped particles (Fig. 2a, inset). Increasing the amount of available ligand up to ligand to metal ratio of 2:1 results in the formation of micron-sized fibres which can reach a length of up to 100 µm with an average thickness of around 1 µm. It can also be seen that each long fibre is made up by a bundle of thinner fibres (Fig. 2b, inset). Furthermore some of the fibres are broken which might be a result of the sonication or spin-coating process. A further increase of the ligand concentration up to a ligand to metal ratio of 3:1 results in the formation of a porous 3-dimensional network (Fig. 2c). The formation of one-dimensional particles such as rods or fibres cannot be observed anymore.

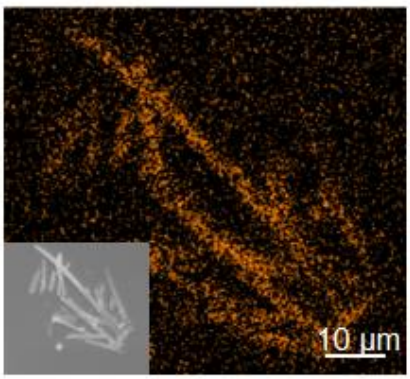

Figure 3: EDX map for Eu(III) and related SEM image (inset) for the micron-sized fibres obtained by ligand to metal ratio of 2:1.

To prove the presence of Eu(III) metal ions in all three samples, energy-dispersive X-ray (EDX) maps were obtained. For the micron-sized fibres obtained in a ligand-to-metal ratio of 2:1 it can be clearly seen that europium atoms can be detected throughout the fibre structure and the shape of the obtained EDX maps are in agreement with the shape of the related SEM image (Fig. 3). Similar results for the EDX mapping were obtained for the cross-shaped micron-sized particles obtained in a ligand to metal ratio of 1:1 (Fig. 4) where the EDX maps for carbon and europium are consistent with the related SEM image.

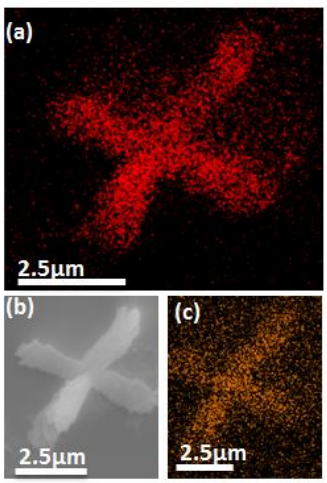

Figure 4: EDX maps for carbon (a) and europium (c) as well as the related SEM image (b) for the cross-shaped particles obtained in a ligand to metal ratio of 1:1.

To further investigate the formation of a coordination polymer the morphologies of the samples were investigated using emission microscopy upon excitation of the samples at 330 - 380 nm and all samples showed a bright red emission (Fig. 5). The microscope images were recorded without background light and the shape observed from the emission images confirms the morphology of the samples from the microscope images without the excitation light. Since direct excitation of Ln(III) metal ions are forbidden, a sensitizer, typically an organic ligand, is required which absorbs light and transfers energy to the Ln(III) metal centres to result in the typical lanthanide emission peaks. The fact that we can observe bright red luminescence upon excitation of the ligand proves that the ligand is coordinated to the metal ion. Furthermore, the red emission can be

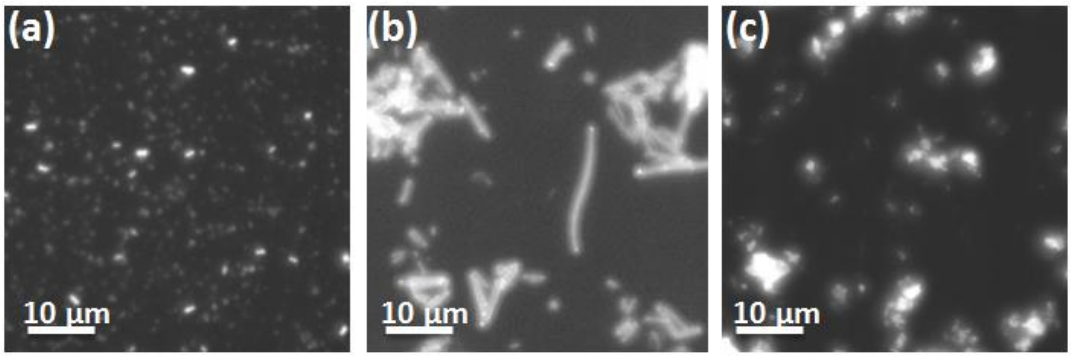

Figure 5: Microscope emission images of excited samples (λ_{ex} = 330 – 380 nm) in in the solid state: (a) ligand to metal ratio 1:1, (b) ligand to metal ratio 2:1, (c) ligand to metal ratio 3:1.

observed throughout the particles in different morphologies indicating that the Eu(III) metal ions are well distributed within the samples. Interestingly the ends of the micron-sized fibres in the microscope emission image for the sample in a ligand to metal ratio of 2:1 (Fig. 5b), appear to be brighter than the centre of the fibre which gives a first indication of wave-guiding properties of the fibres that will be discussed later on in this article.

The changes in the morphology at different ligand to metal ratios can be explained by the self-assembly process between the Eu(III) metal ions and the terpyridine-based ditopic ligand in solution. It should be noted that for the monotopic terpyridine ligand, the 3:1 species is less stable in solution than the 2:1 species where two ligands are coordinated to one Ln(III) metal centre.[23,24] This might be due to a steric factor that the terpyridine ligand is too bulky for the coordination around one Ln(III) metal ion. Related tridentate NNN-coordinating ligands such as pyridine-bis-oxazoline (pybox), where instead of two 6-membered pyridine rings as in terpyridine, the ligand coordination environment next to the centre pyridine ring is made up by two 5-membered oxazoline rings, are more stable in their 3:1 species than in the 2:1 species.[25] Since the coordinating sites in the ditopic ligand used herein is the same as for the monotopic pybox ligand we also expect that the formation of a 2:1 species with two ditopic ligands around one Eu(III) metal centre is more favoured than the formation of the 3:1 species. Furthermore, the formation of metallo-polymers using the same terpyridine-based ditopic ligand with transition metals has been studied before in solution and it was found that the coordination bond exhibits a dynamic behaviour e.g. the ligand and metal ions undergo continual exchange until an equilibrium state is reached. In our case using lanthanides instead of transition metals we expect a similar dynamic behaviour in solution during the self-assembly process. The equilibrium might also be affected by the slow partial evaporation used to obtain the solid samples. During the evaporation, the concentration of the coordinated species increases. As a result the size of the assembled structures in solution increases as well until a critical size is reached and the particles precipitate out of solution.

Based on the coordinating behaviour of the ditopic ligand, dynamic equilibrium during the self-assembly, and the morphologies observed by microscopic methods a potential mechanism for the self-assembly process in solution can be proposed (Scheme 2).

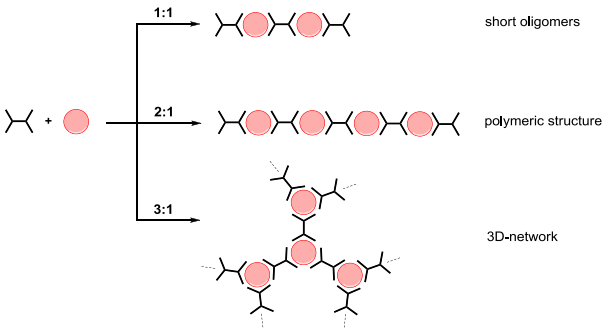

Scheme 2: Proposed mechanism for the self-assembly process in solution at different ligand to metal ratios.

At low ligand to metal ratios of 1:1 and 2:1 used for the self-assembly process in solution, a two-dimensional growth is preferred due to the higher stability of the species with two ditopic ligands coordinated to one metal. In case of an equal ligand to metal ratio of 1:1 the equilibrium between the ligand and the metal is not shifted towards the formation of longer polymeric structures and instead the formation of shorter oligomer chains is preferred. At a higher ligand to metal ratio of 2:1 the additional amount of ligand shifts the equilibrium towards the formation of longer polymeric structures. When a ligand to metal ratio of 3:1 is reached the barrier for the formation of a three-dimensional network were three ligands are coordinated to one Eu(III) metal ion seems to be overcome and thus no one-dimensional polymers can be observed.

Photophysical properties

The photophysical properties of all three Eu(III) containing metallo-supramolecular polymers in different ligand to metal ratios were investigated by steady-state and time-resolved emission spectroscopy. Time-gated emission spectra obtained using a delay of 0.5 ms (1 ms gate) showed typical Eu(III) emission spectra with $^5D_0 \rightarrow {}^7F_J$ (J = 0 – 4) transition lines located at 579, 592, 616, 650, and 689 nm respectively (Figure 6).[16] The branching ratios of emission intensities at the five different emission lines are represented in Table 3. The emission spectrum of all samples exhibits a single symmetrical $^5D_0 \rightarrow {}^7F_0$ transition which contributes around 1 to 2 % to the total emission intensity. The presence and the shape of this transition line indicates that the emission comes from a single species and that the symmetry around the Eu(III) metal ions is at a non-centrosymmetric site.[26]

Table 3: Branching ratios for the emission intensities of $^5D_0 \rightarrow {}^7F_J$ transitions and relative intensity ratios for the $^5D_0 \rightarrow {}^7F_2$ / $^5D_0 \rightarrow {}^7F_1$ transitions for the samples in different ligand to metal ratios.

Ligand / metal ratio	Branching ratio of $^5D_0 \rightarrow {}^7F_J$ / %[a]					Intensity ratio $^7F_2$ / $^7F_1$[b]
	$^7F_0$	$^7F_1$	$^7F_2$	$^7F_3$	$^7F_4$	
1:1	1.5	25.8	51.3	1.5	19.9	1.9
2:1	1.2	16.7	66.1	1.3	14.7	3.9
3:1	0.7	12.4	58.0	0.7	28.2	4.7

[a]Calculated from the integrated intensities of the emission spectra, [b]calculated from the relative $^5D_0 \rightarrow {}^7F_2$ and $^5D_0 \rightarrow {}^7F_1$ branching ratios.

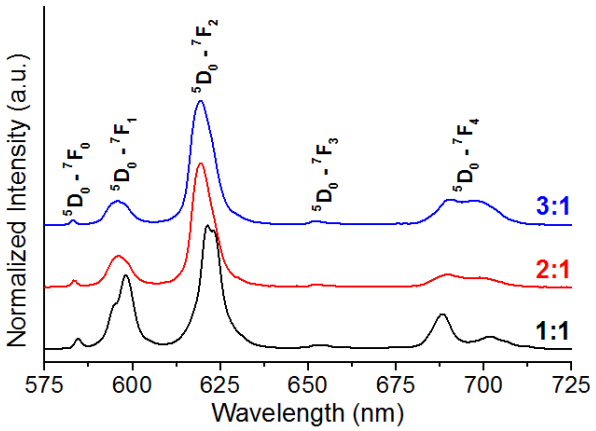

Figure 6: Time-gated emission spectra (0.5 ms delay, 1 ms gate) for all three samples with different ligand to metal ratios.

For all three samples the transition which has the highest contribution to the overall emission intensity is the $^5D_0 \rightarrow {}^7F_2$ line (616 nm), a hypersensitive transition whose intensity strongly depends on the symmetry around the Eu(III) metal centre. In comparison, the magnetic dipole allowed $^5D_0 \rightarrow {}^7F_1$ transition (592 nm) does not depend on the Eu(III) symmetry and as a result the difference of the $^5D_0 \rightarrow {}^7F_2$ and $^5D_0 \rightarrow {}^7F_1$ emission intensity ratios can be used to obtain information about the Eu(III) site symmetry of the samples.[27] Herein the obtained emission intensity ratio constantly increases from about two at a ligand to metal ratio of 1:1 to about five at a ligand to metal ratio of 3:1, indicating a lowering of the symmetry order with an increase of the ligand to metal ratio.[28]

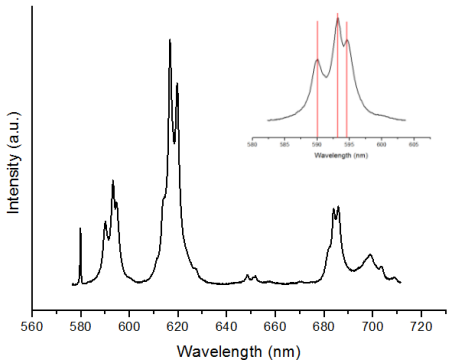

Figure 7: Higher resolution emission spectrum of the sample in a ligand to metal ratio of 1:1 and splitting pattern of the Eu (III) $^5D_0$-$^7F_1$ transition (inset).

To further investigate the symmetry around the Eu(III) metal centre, we recorded higher resolution emission spectra to resolve crystal field splitting of the different transitions. In case of the sample in a ligand to metal ratio of 1:1 it can be seen at higher resolution that the $^5D_0 \rightarrow {}^7F_1$ transition actually splits into two main transitions located at around 590 nm and 594 nm. (Fig. 7) which suggests a Eu(III) D_3 site symmetry.[29] The splitting corresponds to Eu(III) $^7F_1$ ligand-field sublevels at 293 cm^{-1} (irreducible representation A in D_3) and 430 cm^{-1} (irreducible representation E in D_3) whereby the energy difference (ΔE(A-E) = 137 cm^{-1}) is proportional to the ligand field strength. Furthermore, an additional splitting for $^7F_1$(E) (ΔE(E-E) = 41 cm^{-1}) can be seen at 594 nm which represents the distortion from the ideal D_3 symmetry and we therefore conclude that in this sample the Eu(III) metal ion symmetry is pseudo-D_3. The obtained results are comparable to a reported homoditopic ligand Eu(III) complex which has also been found to show an emission spectrum and splitting pattern according to a pseudo-D_3 symmetry.[30] For samples at ligand to metal ratio of 2:1 and 3:1 the $^5D_0 \rightarrow {}^7F_1$ line is broader than for the sample in a 1:1 ratio and no splitting pattern could be observed. However, as one can see from Figure 6 and Table 3, the overall shape of the emission spectra show significant differences (especially for the $^5D_0 \rightarrow {}^7F_4$ transition) compared to the sample in a ligand to metal ratio of 1:1 with a pseudo-D_3 symmetry. We therefore conclude that the symmetry for these two samples must be different, presumably other lower order symmetry point groups such as C_3 or C_{2V}.[29] However, the changes of the emission spectra show that all three samples in different ligand to metal ratios have a different coordination environment and site symmetry around the Eu(III) metal centre. This is consistent with the morphology changes found using SEM as well as the findings from elemental analysis which showed a larger number of coordinated ligands with increases in the ligand to metal ratio.

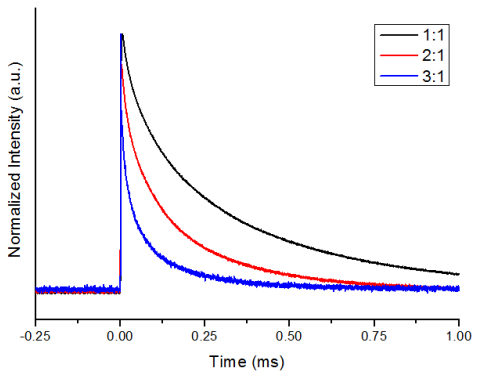

Figure 8: Emission decay curves for the Eu(III) $^5D_0$-$^7F_2$ transition measured at 616 nm for different ligand to metal ratios.

The time-resolved emission decay curves were recorded for the most prominent Eu(III) $^5D_0$-$^7F_2$ transition located at 616 nm (Fig. 8). All decay curves can be fitted to bi-exponential decay functions indicating that in all samples at least two different Eu(III) emitting species are present (Table 4). The longer of the obtained decay times is in the ms range, which is typical for Eu(III) emissive compounds in the solid state, while the second shorter decay time is in the µs range.

Table 4: Emission decay times and relative contribution of the Eu(III) $^5D_0$-$^7F_2$ transition measured at 616 nm for different ligand to metal ratios.

	τ_1 / ms	A_1 / %	τ_1 / ms	A_2 / %	τ / ms[a]
1:1	0.48	59	0.09	41	0.44
2:1	0.30	49	0.07	51	0.26
3:1	0.18	42	0.04	58	0.15

[a]Average lifetime obtained using equation: $\tau = (A_1\tau_1^2 + A_2\tau_2^2)/(A_1\tau_1 + A_2\tau_2)$.

It should be noted that an increase of the ligand to metal ratio from 1:1 to 3:1 leads to significant changes of both decay times and their relative contribution to the average lifetime. Firstly an increase of the ligand to metal ratio results in a decrease of the relative contribution A_1 and an increase of A_2 indicating that at higher ligand to metal ratios

the percentage of shorter living species is higher. Secondly, an increase of the ligand to metal ratio results in a shortening of both longer and shorter decay times, as well as a shortening of the average lifetime from 0.44 ms at a ligand to metal ratio of 1:1 to about 0.15 ms at a ligand to metal ratio of 3:1. This result is rather surprising because the coordination of more ligand to the Eu(III) metal centres was expected to result in a more shielded Eu(III) metal environment which should prevent quenching pathways such as by coordinated water molecules. As a result the lifetime should be increasing with higher ligand to metal ratios. However, in the case of the ditopic tridentate terpyridine ligand used herein, a shortening of the lifetime with increasing coordination of ligand can be observed which could be explained by a possible ligand quenching pathway introduced by some ligand moieties such as C-H vibrations.[31,32]

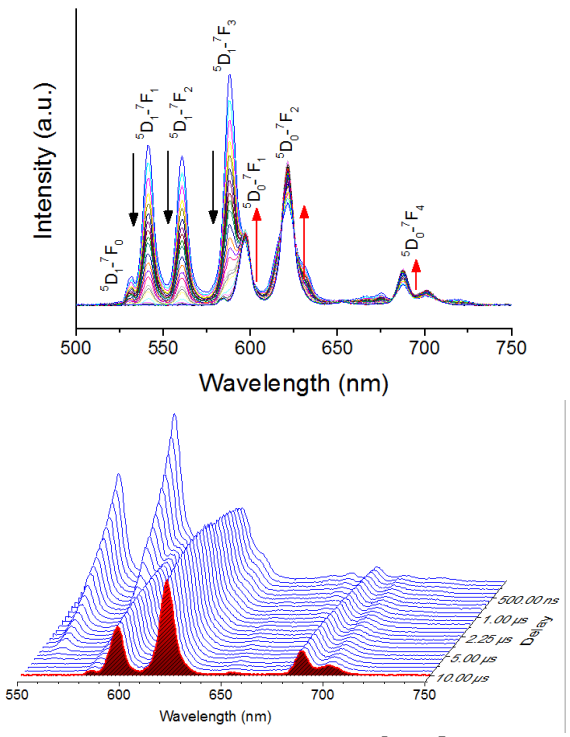

Figure 9: Time-gated emission maps for the $^5D_1 - {}^7F_J$ (J = 0 – 3) and $^5D_0 - {}^7F_J$ (J = 0 -4) transition recorded between 100 ns and 10 µs (500 ns gate, 2 nm band width).

Next to the Eu(III) $^5D_0$ state (17500 cm^{-1}), emission can also occur from the Eu(III) $^5D_1$ state located at higher energies (19500 cm^{-1}). To get a deeper understanding of the energy transfer process from the ligand to the Eu(III) metal centres, time-gated emission maps from the $^5D_1$ state in the early stage of the Eu(III) emission were obtained (Fig. 9). The spectra for all samples showed the characteristic $^5D_1 \rightarrow {}^7F_J$ (J = 0 -3) transition lines located at 526, 537, 555, and 583 nm respectively.[33] Time-gated emission maps of the Eu(III) emission between 100 ns and 10 µs with a time gate of 500 ns as well as the related emission decay curves showed that the lifetime of the $^5D_1 \rightarrow {}^7F_J$ emission lines is in the µs range which is much shorter than the ms range of the $^5D_0 \rightarrow {}^7F_J$ emission (Fig. 10). The $^5D_1 \rightarrow {}^7F_J$ emission lifetimes for all three samples are shown in Table 5 and it can be seen that the value is decreasing from 1.2 µs at a ligand to metal ratio of 1:1 to 0.8 µs and 0.6 µs at ligand to metal ratios of 2:1 and 3:1 respectively. Furthermore, the $^5D_1 \rightarrow {}^7F_J$ emission lifetimes increase significantly upon cooling to 77 K and become very similar for all three samples. It should be noted that the $^5D_0 \rightarrow {}^7F_2$ emission decay time does not change at 77 K compared to measurements at 295 K.

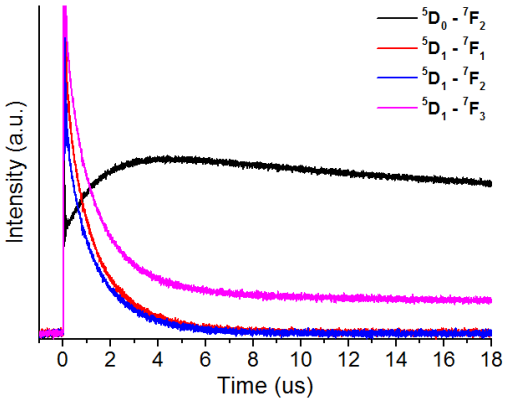

Figure 10: $^5D_1$-^7F_J (J = 0 – 3) emission and $^5D_0$-$^7F_2$ decay curves for a sample in a ligand to metal ratio of 1:1.

Table 5: $^5D_1$-^7F_J (J = 0 – 3) emission decay times and $^5D_0$-$^7F_2$ emission rise times in the early stage at 295 K and 77 K, relative population of $^5D_0$ state by the $^5D_1$ state, and triplet state energies for the samples in different ligand to metal ratios.

Ligand / metal ratio	τ / µs			$^5D_1$-$^5D_0$ / %	E (^{3}T) / cm^{-1} [(b)]
	$^5D_1$-^7F_J 295 K	$^5D_0$-$^7F_2$ 295 K[(a)]	$^5D_0$-$^7F_2$ 77 K		
1:1	1.2	1.2	1.7	39	22021
2:1	0.8	0.7	1.5	29	20709
3:1	0.6	0.5	1.6	22	20401

[(a)] Signal rise times fitted from the overall $^5D_0 - {}^7F_2$ emission decay curves between 0 and 5 µs, [(b)] calculated from the highest energy peak obtained by Gaussian fitting of the phosphorescence spectra.

Interestingly a rise of the $^5D_0 \rightarrow {}^7F_2$ emission intensity on the same timescale can be seen. For all three samples, the emission decay time values for the $^5D_1 \rightarrow {}^7F_J$ (J = 0 -3) transitions are very similar to the emission rise time values of the $^5D_0 \rightarrow {}^7F_2$ transition (Table 5) which suggests that the $^5D_0$ state is partly populated via relaxation from the $^5D_1$ excited state. The relative contribution of this process to the initial population of the $^5D_0$ state can be estimated from the time profile of emission at $^5D_0 \rightarrow {}^7F_2$ transition line (e.g. Fig.10 for 1:1 ratio). Value of the emission intensity at this line at time zero, I_0, is proportional to the population of $^5D_0$ formed by direct energy transfer from the ligand triplet state. Further increase in the emission intensity up to the maximum intensity, I_{max}, should be assigned to the increase in $^5D_0$ population due to the relaxation from the $^5D_1$ state because its rise time is equal to the decay time $^5D_1 \rightarrow {}^7F_J$ (J = 0 -3) transitions. Therefore, the relative contribution of the relaxation from $^5D_1$ to $^5D_0$ to the initial population of $^5D_0$ can be simply estimated as $1-I_0/I_{max}$ (taking into account that $^5D_0$ decay time is significantly longer than the rise time of its population). It was found that upon increasing the ligand to metal ratio this contribution decreased from about 39 % at a ligand to metal ratio of 1:1 to about 29 % and 22 % at ligand to metal ratios of 2:1 and 3:1 respectively.

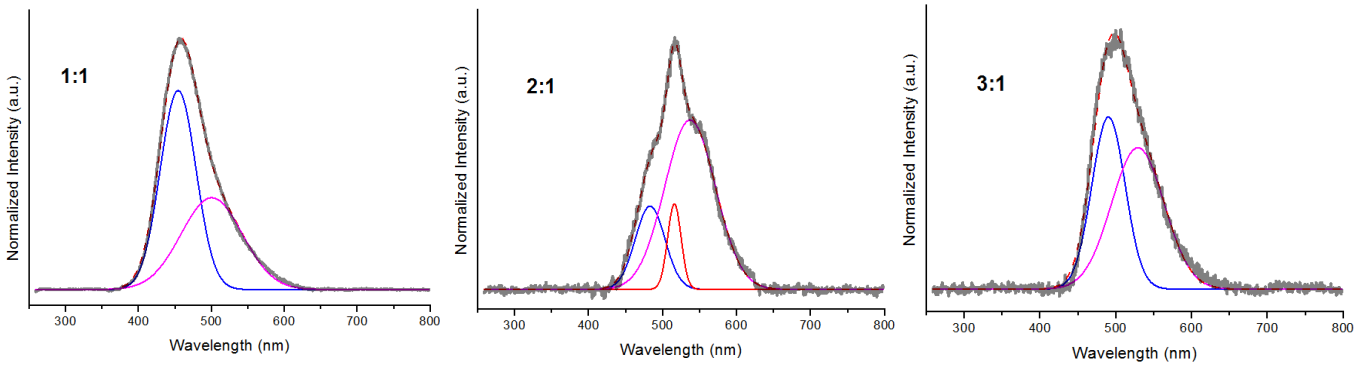

Figure. 11: Phosphorescence spectra and Gaussian peak fitting of the Gd(III) samples in different ligand to metal ratios (100 µs delay, 1 ms gate, 2 nm band), blue colour lines correspond to highest energy peaks.

The influence of the ligand to metal ratio used during the self-assembly process in solution on the triplet state energies of the ligand in the solid state was investigated by measurements of phosphorescence spectra of the related Gd(III) samples in the solid state at 77 K (Fig. 11). The phosphorescence spectra were fitted using Gaussian peak fitting and the wavelengths for the highest energy peaks were used to determine the triplet state energy for each sample. It was found that the triplet state energy of the ligand significantly decreases from about 22021 cm^{-1} at a ligand to metal ratio of 1:1 to about 20709 cm^{-1} at a ligand to metal ratio of 2:1.

The triplet state energy of the sample in a ligand to metal ratio of 3:1 (20401 cm^{-1}) is similar to the 2:1 sample. The lowering of the triplet state energy correlates well with the decrease of the $^5D_1 \rightarrow {}^7F_J$ (J = 0 -3) emission decay times as well as the population contribution of the $^5D_0$ state by the $^5D_1$ state at room temperature. The energy difference between the Eu(III) $^5D_1$ state (19500 cm^{-1}) and the triplet state energies of the ligand for the samples in ligand to metal ratios of 2:1 and 3:1 is only around 1000 cm^{-1} and as a result energy back transfer from the $^5D_1$ state to the ligand triplet state can occur at room temperature. At 77 K no energy back transfer can occur and therefore the $^5D_0 - {}^7F_2$ rise times as well as the population contribution of the $^5D_0$ state by the $^5D_1$ state are in a similar range for all the samples

Optical wave-guiding properties

Earlier we discussed that emission from the ends of the micron-sized fibres, obtained in a ligand to metal ratio of 2:1, appear to be brighter than the other parts of the fibre upon UV-excitation (Figure 5b). To further investigate the optical wave-guiding properties we performed the following experiment. Under a microscope an isolated fibre was chosen and one end of the fibre was illuminated using 355 nm laser light focussed in a 2 µm spot size (Fig. 12). Images of the fibre upon excitation were taken with and without a 355 nm long pass filter which efficiently removed scattered laser radiation (Fig. 12, inset). The illuminated area shows bright red emission which results from the Eu(III) metal centres of the metallo-polymers. Additionally Eu(III) emission can be seen on the other end of the fibre which is not illuminated by laser light. It should be noted that the emission from the walls of the fibres outside the irradiated area is much less compared to the end of the fibre. We therefore conclude that emission of this end of the fibre arrives from rather efficient optical wave-guiding of emission excited from the other end of the fibre. The laser power dependence of the emission of this end of the fibre follows a linear trend suggesting that the nature of the emission observed is rather spontaneous than stimulated. This is expected with continuous wave irradiation. Furthermore, these optical wave-guiding properties can be seen as a proof of the continuity of the fibre medium.

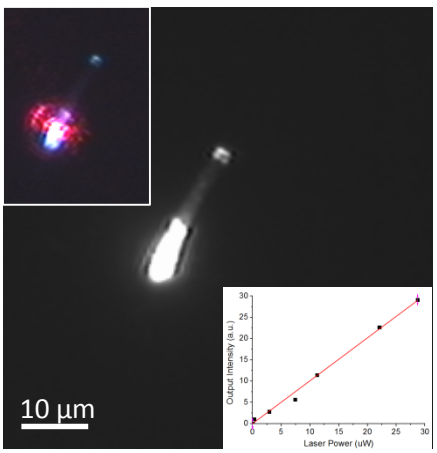

Figure 12: Optical wave-guiding properties of the fibres obtained in a ligand to metal ratio of 2:1 and power dependence profile of the emission (inset).

Conclusions

In conclusion, we have reported the formation of supramolecular polymers between a ditopic terpyridine-based ditopic ligand and Eu(III) metal ions in the solid state. We further showed that the morphology of these metallo-polymers strongly depends on the ligand to metal ratio used during the solution phase self-assembly process whereby the morphology can be controlled from one-dimensional micron-sized fibres to a three-dimensional coordination network. All samples prepared herein show a strong bright characteristic red emission upon UV-excitation indicating that the ligand used herein can also act as an efficient sensitizer for Eu(III) emission. The energy transfer process for the Eu(III) emission was further investigated by emission lifetime kinetics of the rarely observed $^5D_1$-^7F_J transition as well as phosphorescence spectra of the related Gd(III) samples. Next to the morphology of the samples the ligand triplet state energies, derived from the phosphorescence spectra, show a strong dependence on the ligand to metal ratio. Furthermore, the micron-sized fibres obtained at a ligand to metal ratio of 2:1, can act as efficient optical wave-guides. To our knowledge this is the first example of optical wave-guiding fibres which consist of coordination supramolecular polymers derived from a self-assembly process in solution. Such optical wave-guides can be used for optical signal transmission, concentration of emissive light in a small region, and potential amplified spontaneous emission sources. Lanthanide emission is especially suited for many such applications due to the low emission losses due to self-absorption since the red emission is greatly shifted from the ligand or metal absorption.

Notes and references

[a] Department of Chemistry, National University of Singapore, 3 Science Drive 3, Singapore 117543

[b] Institute of Materials Research and Engineering (IMRE), Agency for Science, Technology & Research (A*STAR), 3 Research Link, Singapore 117602 (andyhor@imre.a-star.edu.sg)

[c] Department of Chemistry, Imperial College London, London, SW7 2AZ, UK (n.long@imperial.ac.uk)

[d] Department of Chemistry, University Brunei Darussalam, Jalan Tungku Ling, Gadong BE 1410, Brunei

1 L. Yang, X. Tan, Z. Wang and X. Zhang, *Chem. Rev.*, 2015, in press, 10.1021/cr500633b.
2 A. Ustinov, H. Weissman, E. Shirman, I. Pinkas, X. Zuo and B. Rybtchinski, *J. Am. Chem. Soc.*, 2011, **133**, 16201–11.
3 S. Burattini, B. W. Greenland, D. H. Merino, W. Weng, J. Seppala, H. M. Colquhoun, W. Hayes, M. E. Mackay, I. W. Hamley and S. J. Rowan, *J. Am. Chem. Soc.*, 2010, **132**, 12051–8.
4 E. Kolomiets, E. Buhler, S. J. Candau, J. Lehn, L. D. C. and L. Pasteur, *Macromolecules*, 2006, **39**, 1173–81.
5 V. A. Friese and D. G. Kurth, *Coord. Chem. Rev.*, 2008, **252**, 199–211.
6 V. A. Friese and D. G. Kurth, *Curr. Opin. Colloid Interface Sci.*, 2009, **14**, 81–93.
7 Y. Zhou, M. Hong and X. Wu, *Chem. Commun.*, 2006, 135–43.
8 M. Higuchi, *J. Mater. Chem. C*, 2014, **2**, 9331–41.
9 F. S. Han, M. Higuchi, T. Ikeda, Y. Negishi, T. Tsukuda and D. G. Kurth, *J. Mater. Chem.*, 2008, **18**, 4555.
10 B. Angulo, J. I. Garc, C. I. Herrer, J. A. Mayoral and A. C. Min, *J. Org. Chem.*, 2012, **77**, 5525–32.
11 D. G. Kurth and M. Higuchi, *Soft Matter*, 2006, **2**, 915–927.
12 J. R. Kumpfer, J. Jin and S. J. Rowan, *J. Mater. Chem.*, 2010, **20**, 145–151.
13 M. Chiper, R. Hoogenboom and U. S. Schubert, *Macromol. Rapid Commun.*, 2009, **30**, 565–78.
14 R. Dobrawa, M. Lysetska, P. Ballester, M. Gru and F. Wu, *Macromolecules*, 2005, **38**, 1315–25.
15 C. Hu, T. Sato and J. Zhang, *ACS Appl. Mater. …*, 2014, **6**, 9118–25.
16 J.-C. G. Bünzli and C. Piguet, *Chem. Soc. Rev.*, 2005, **34**, 1048–77.
17 V. Bekiari and P. Lianos, *Adv. Mater.*, 2000, **12**, 1603–05.
18 V. Bekiari and P. Lianos, *Journal of Luminescence*, 2003, **101**, 135–40.
19 T. Vermonden, W. M. de Vos, A. T. M. Marcelis and E. J. R. Sudhölter, *Eur. J. Inorg. Chem.*, 2004, 2847–52.
20 E. C. Constable and A. M. W. C. Thompson, *Dalt. Trans.*, 1992, **2**, 3467–75.
21 M. Higuchi, Y. Otsuka, R. Shomura and D. G. Kurth, *Thin Solid Films*, 2008, **516**, 2416–20.
22 L. Xu, L. Feng, Y. Han, Y. Jing, Z. Xian, Z. Liu, J. Huang and Y. Yan, *Soft Matter*, 2014, **10**, 4686–93.
23 A. Chauvin, F. Gumy, D. Imbert and J. G. Bünzli, *Spectrosc. Lett.*, 2004, **37**, 517–32.
24 H.-R. Mürner, E. Chassat, R. P. Thummel and J.-C. G. Bünzli, *J. Chem. Soc. Dalt. Trans.*, 2000, 2809–16.
25 A. de Bettencourt-Dias, P. S. Barber, S. Viswanathan, D. T. de Lill, A. Rollett, G. Ling and S. Altun, *Inorg. Chem.*, 2010, **49**, 8848–61.
26 P. A. Tanner, *Chem. Soc. Rev.*, 2013, **42**, 5090–101.
27 P. Zhang, Y. Wang, H. Liu and Y. Chen, *J. Mater. Chem.*, 2011, **21**, 18462–66.
28 S. Tang, A. Babai and A.-V. Mudring, *Angew. Chem. Int. Ed. Engl.*, 2008, **47**, 7631–4.
29 J. Kang and T. Kim, *Bull. Korean Chem. Soc.*, 2005, **26**, 1057–64.
30 E. Deiters, B. Song, A.-S. Chauvin, C. D. B. Vandevyver, F. Gumy and J.-C. G. Bünzli, *Chemistry*, 2009, **15**, 885–900.
31 G. Stein, *J. Chem. Phys.*, 1975, **62**, 208–213.
32 Y. Zheng, M. Motevalli, R. H. C. Tan, I. Abrahams, W. P. Gillin and P. B. Wyatt, *Polyhedron*, 2008, **27**, 1503–1510.
33 R. Brennetot and J. Georges, *Spectrochim. Acta Part A Mol. Biomol. Spectrosc.*, 2000, **56**, 703–715.

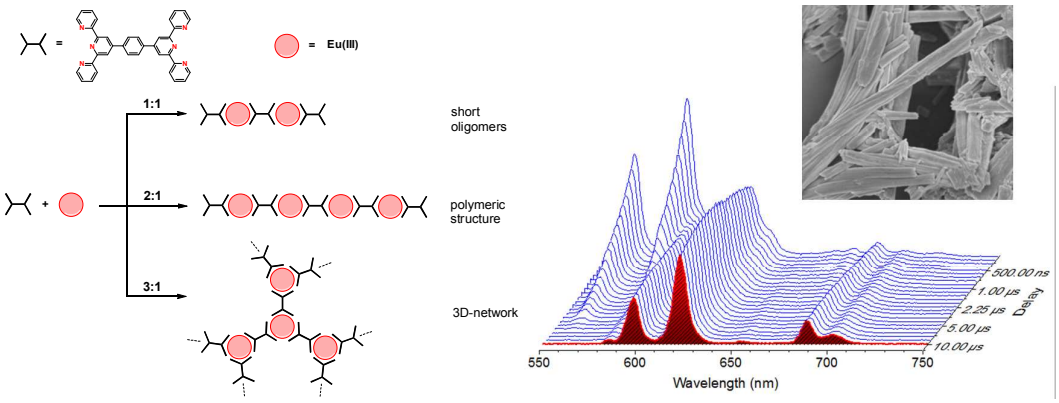

Preparation, photophysical studies, and optical wave-guiding properties of morphology controllable Eu(III) containing coordination polymers in the solid state.